A Waveguide Directional Coupler with a Nonlinear Coupling Medium

Paul R. Berger, *Member, IEEE,* Pallab K. Bhattacharya, *Fellow, IEEE,* and Shantanu Gupta

Abstract—**An all-optical switch using a waveguide directional coupler with a nonlinear coupling medium is shown. At low input power, it performs as a linear directional coupler; but at higher input powers, the coupling length increases, thus reducing coupling. For coupling lengths near multiples of the linear coupling length, switching can occur from a crossed-over state at low power to a straight-through condition at higher input power. Theoretical analysis which describes the behavior is developed. A nonlinear coupler was fabricated which exhibited switching at 45.6 meV below the exciton resonance with a critical intensity of 3×10^4 W/cm^2. Modeling of the device shows that $n_2 = 1.88 \times 10^{-8}$ cm^2/W and $\alpha = 12.9$ cm^{-1}.**

I. Introduction

THERE is great interest in the development of an active low power optical switch which would potentially be much faster than conventional electronic devices. An all-optical switch made using a nonlinear waveguide directional coupler was first proposed by Jensen [1]. Such a device would be made entirely of nonlinear medium and operate as a linear directional coupler at low input power. However, at higher input powers, optical nonlinearities create a modification in the phase matching of both waveguides. Eventually, a detuning from the low power coupling condition is achieved. A nonlinear coupler, whose length is equal to one linear coupling length (L_c), will show complete transfer of power at low powers but will achieve a straight-through, or back-coupled condition in which no light is transferred at higher input powers.

Li Kam Wa *et al.* [2]–[5] first demonstrated switching with change in power using such a nonlinear directional coupler made entirely of a GaAs/AlGaAs multiple quantum well (MQW). To obtain large switching at low powers, a high nonlinearity is desired. Nonlinearity can be increased in MQW structures over bulk due to enhanced excitonic absorption [6]. Also, the nonlinearity can be increased by operating at light wavelengths closer to band edge. However, absorption losses increase, too. In the device demonstrated by Li Kam Wa *et al.* [2]–[5], absorption takes place in all regions of the device. Cada *et al.* [7]–[9] proposed a nonlinear coupler which used a nonlinear medium *only* in the active coupling region to reduce the loss. This device could therefore be operated closer to the band edge with subsequent higher nonlinearity but maintaining a reasonable loss. The first demonstration of such a vertical nonlinear coupler was made by us [10], but the guides were multimode and asymmetric. In this paper, we demonstrate nonlinear switching of a single-mode and symmetrical coupler, and have also analyzed its switching behavior. Section II describes the analysis and calculated behavior of our coupler. Sections III and IV describe the experimental techniques and results; and conclusions are made in Section V.

Manuscript received March 20, 1990; revised July 10, 1990. This work was supported by the Army Research Office under Contracts DAAL03-87-K0007 and DAAL03-86-K0105.

P. R. Berger is with AT&T Bell Laboratories, Murray Hill, NJ 07974.

P. Bhattacharya and S. Gupta are with the Department of Electrical Engineering and Computer Science, University of Michigan, Ann Arbor, MI 48109.

IEEE Log Number 9143390.

II. Theoretical Calculations

A. Linear Directional Coupler

The linear coupling behavior was modeled by treating the directional coupler as slab waveguides, as shown in Fig. 1, and solving for the electric field amplitude, $\mathcal{E}(x)$, in each of the five regions shown below in (1), following the analysis of Marcuse [11]. Only the TE modes were considered since, for our experiments, only the TE mode is excited.

$$\mathcal{E}(x) = \begin{cases} A_1 \exp\left[-\gamma_1(x - S_3 - d_2)\right] \\ \qquad x \geq S_3 + d_2 \\ A_2 \cos\left[k_2\left(x - S_3 - \frac{d_2}{2}\right)\right] \\ \quad + A_3 \sin\left[k_2\left(x - S_3 - \frac{d_2}{2}\right)\right] \\ \qquad S_3 + d_2 \geq x \geq S_3 \\ A_4 \exp\left[-\gamma_3 x\right] + A_5 \exp\left[\gamma_3 x\right] \\ \qquad -S_3 \leq x \leq S_3 \\ A_6 \cos\left[k_4\left(x + S_3 + \frac{d_4}{2}\right)\right] \\ \quad + A_7 \sin\left[k_4\left(x + S_3 + \frac{d_4}{2}\right)\right] \\ \qquad -S_3 \leq x \leq -(S_3 + d_4) \\ A_8 \exp\left[\gamma_5(x + S_3 + d_4)\right] \\ \qquad x \leq -(S_3 + d_4). \end{cases} \tag{1}$$

The A_i's are constants and the parameters k_i and γ_i are given by

$$k_i^2 = (n_i^2 k^2 - \beta^2) \qquad i = 2, 4 \tag{2}$$

$$\gamma_i^2 = (\beta - n_i^2 k^2) \qquad i = 1, 3, 5 \tag{3}$$

where β is the propagation constant of the guided modes, and $k_0 = 2\pi/\lambda$ is the free space propagation constant.

By employing boundary conditions that the electric field must be continuous and smooth at each interface, a series of eight equations with eight unknown A_i coefficients is generated, as shown in matrix form

Cladding	n_1	
Slab 1	n_2	d_2 ⇕
Coupling	n_3	$2S_2$ ⇕
Slab 2	n_4	d_4 ⇕
Cladding	n_5	

Fig. 1. Schematic of the five regions of a slab directional coupler.

$$M = \begin{bmatrix} 1 & -\cos\left(\frac{d_2k_2}{2}\right) & -\sin\left(\frac{d_2k_2}{2}\right) & 0 & 0 & 0 & 0 & 0 \\ -\gamma_1 & k_2\sin\left(\frac{d_2k_2}{2}\right) & -k_2\cos\left(\frac{d_2k_2}{2}\right) & 0 & 0 & 0 & 0 & 0 \\ 0 & \cos\left(\frac{d_2k_2}{2}\right) & -\sin\left(\frac{d_2k_2}{2}\right) & -e^{-\gamma_3S_3} & -e^{\gamma_3S_3} & 0 & 0 & 0 \\ 0 & k_2\sin\left(\frac{d_2k_2}{2}\right) & k_2\cos\left(\frac{d_2k_2}{2}\right) & -\gamma_3S_3 & -\gamma_3e^{\gamma_3S_3} & 0 & 0 & 0 \\ 0 & 0 & 0 & e^{\gamma_3S_3} & e^{-\gamma_3S_3} & -\cos\left(\frac{d_4k_4}{2}\right) & -\sin\left(\frac{d_4k_4}{2}\right) & 0 \\ 0 & 0 & 0 & -\gamma_3e^{\gamma_3S_3} & \gamma_3e^{-\gamma_3S} & k_4\sin\left(\frac{d_4k_4}{2}\right) & -k_4\cos\left(\frac{d_4k_4}{2}\right) & 0 \\ 0 & 0 & 0 & 0 & 0 & \cos\left(\frac{d_4k_4}{2}\right) & -\sin\left(\frac{d_4k_4}{2}\right) & -1 \\ 0 & 0 & 0 & 0 & 0 & k_4\sin\left(\frac{d_4k_4}{2}\right) & k_4\cos\left(\frac{d_4k_4}{2}\right) & -\gamma_5 \end{bmatrix} \quad (4)$$

The determinant of the matrix is then set to zero

$$|\det M| = 0 \quad (5)$$

to yield the eigenvalues of β. For single-mode waveguides, there are two solutions for the linear directional coupler, β_1 and β_2, which represent an even and odd supermode of the coupler. To solve for the amplitude coefficients (A_i) of the five regions, we set $A_1 = 1$ and solve for the other A_i coefficients proportionally scaled to $A_1 = 1$. Fig. 2 shows the electric field solution of the even and odd supermodes. For the calculations, the following values were used: $n_1 = n_5 = 3.4576$, $n_2 = n_4 = 3.5336$, $n_3 = 3.5006$, $d_2 = d_4 = 0.8\ \mu$m, $S_3 = 0.6\ \mu$m, and $\lambda = 0.8118\ \mu$m. Refractive index data were obtained from calculations reported by Adachi [12]. Coupling of light occurs from a superposition of these even and odd supermodes, where the coupling length is given by

$$L = \frac{\pi}{|\beta_2 - \beta_1|}. \quad (6)$$

The relative intensity switching of the coupler is shown in Fig. 3 at the given lengths (a) 0.0, (b) $0.5 \times L_c$, and (c) L_c by using the supermodes of Fig. 2. The linear analysis yields two important design considerations. First, the evanescent tail is sufficiently quenched in regions 1 and 5. If the tail is significant to penetrate through regions 1 and 5, then the coupler will become detuned due to the asymmetry of one side facing the substrate and the other side air. Second, approximate values for β, the guided mode's propagation constant, and L_c, the linear coupling length are found to aid during the measurements and further nonlinear modeling.

B. Nonlinear Directional Coupler

The basic theory of a nonlinear coupler developed by Jensen [1] models the two individual slab waveguides as decoupled slab waveguides and assumes all five regions are nonlinear. The coupler behavior is modeled with the coupled mode equations below:

$$-i\frac{\partial a_1}{\partial z} = Q_1a_1 + Q_2a_2 + (Q_3|a_1|^2 + 2Q_4|a_2|^2)a_1 \quad (7)$$

and

$$-i\frac{\partial a_2}{\partial z} = Q_1a_2 + Q_2a_1 + (Q_3|a_2|^2 + 2Q_4|a_1|^2)a_2 \quad (8)$$

where a_1 and a_2 are the complex normalized amplitudes of the two modes and $Q_1 - Q_4$ are the coupling coefficients. The coupled mode theory couples the two separate wavguide modes, which are different than the supermodes mentioned in the linear case.

Each term in (7) and (8) can be associated with a particular contribution of the perturbing polarization. The terms involving Q_1 arise from the overlap of the mode field with the adjacent waveguide; they serve only to modify the propagation constant of the mode. The Q_2 terms arise because of the presence of a mode in the adjacent guide and lead to linear coupling between the waveguides. The terms with Q_3 are the strongest nonlinear terms and arise from the nonlinear interaction of a mode with itself. They are equivalent to the self-phase modulation and self-focusing terms in free space nonlinear optics. The terms involving Q_4 arise from the nonlinear interaction of one mode with the mode in the adjacent guide.

The coupled mode equations reduce to the simplified form shown below:

$$\frac{\partial a_1}{\partial z} = -j\beta a_1 - \left(\frac{\alpha}{2}\right)a_1 + jCa_2 - jn_2k_0|a_1|^2a_1 \quad (9)$$

and

$$\frac{\partial a_2}{\partial z} = -j\beta a_2 - \left(\frac{\alpha}{2}\right)\alpha_2 + jCa_1 - jn_2k_0|a_2|^2a_2 \quad (10)$$

where α is the loss coefficient, C is the linear coupling coefficient, and n_2 is the nonlinear refractive index. The solution shown below:

$$a_1 = B_1(z)e^{-j\varphi_1(z)} \quad (11)$$

$$a_2 = B_2(z)e^{-j\varphi_2(z)} \quad (12)$$

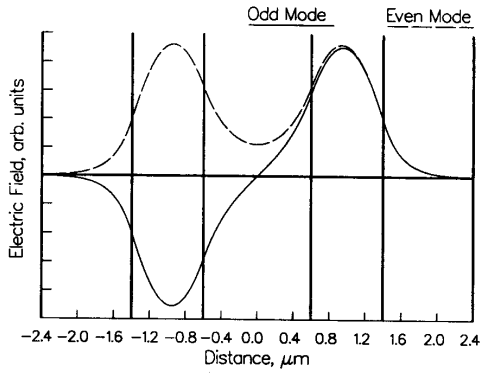

Fig. 2. Electric field profile of the even and odd modes in a five region slab directional coupler.

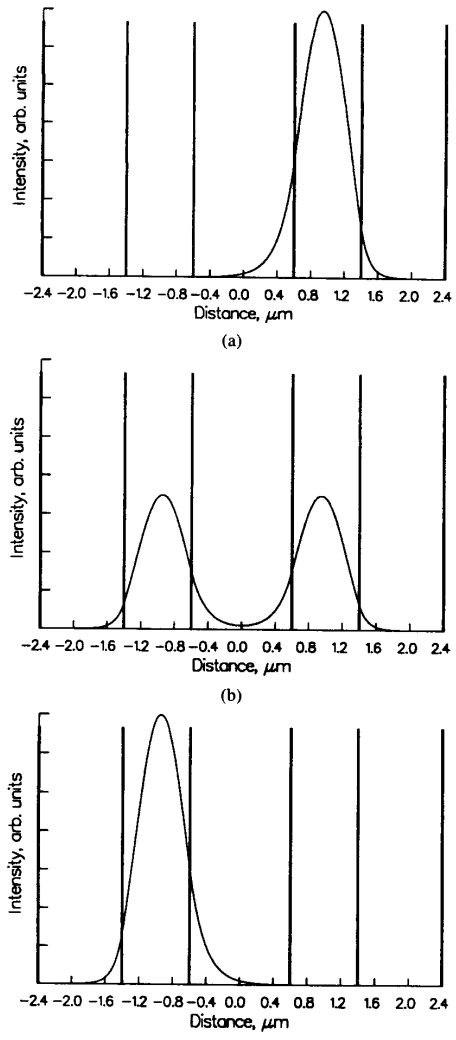

Fig. 3. Intensity profile of a directional coupler at the lengths (a) 0, (b) $0.5 \times L_c$, and (c) L_c.

are assumed and substituted back into (9) and (10), where B_1, B_2, φ_1, and φ_2 are real functions of z. The real and imaginary terms can be separated and the following four equations obtained:

$$\frac{\partial B_1}{\partial z} = -\left(\frac{\alpha}{2}\right) B_1 + CB_2 \sin(\varphi_2 - \varphi_1) \tag{13}$$

$$\frac{\partial B_2}{\partial z} = -\left(\frac{\alpha}{2}\right) B_2 + CB_2 \sin(\varphi_1 - \varphi_2) \tag{14}$$

$$\frac{\partial \varphi_1}{\partial z} = \beta + n_2 k_0 B_1^2 \tag{15}$$

$$\frac{\partial \varphi_1}{\partial z} = \beta + n_2 k_0 B_1^2. \tag{16}$$

Solutions of (9) and (10) show that the nonlinearity manifests itself to modify the phase, φ_1 and φ_2, of the two modes, and therefore destroys the coupling behavior. However, the modeled switching behavior with increasing incident power using Jensen's analysis does not accurately model our experimental data, as will be shown later. For our case, the guide material refractive index is not significantly changing with excitation but only the coupling region refractive index exhibits nonlinearity, as given by

$$n = n_0 - n_2 I. \tag{17}$$

Slight modifications in φ_1 and φ_2 are possible for the case of the coupling region only being nonlinear, as the coupling region refractive index changes the mode confinement. But the major contribution of the nonlinear effect, for the case of linear guides with nonlinear coupling medium, is a decrease in the refractive index of the coupling region MQW and, therefore, a reduction of the evanescent tail into the coupling medium and into the adjacent guide at higher powers. This acts to modulate the coupling coefficient and subsequently the coupling length. For our situation, we will propose that the coupling coefficient is given by the general form

$$C = \frac{\pi}{2L_c} - k_0 n_2 (I_{MQW}) \tag{18}$$

to approximately model the modulation of the coupling coefficient, but is invalid when $C < 0$. The intensity I_{MQW} used is an approximation of power within the coupling region which assumes 10% of the total guided power (I_{tot}), shown below, is within the coupling region (i.e., $I_{MQW} = 0.1 I_{tot}$):

$$I_{tot} = a_1^2 + a_2^2. \tag{19}$$

Absorption effects upon I_{tot} are included in the coupled mode equations which are written as

$$\frac{\partial a_1}{\partial z} = -j\beta a_1 - \left(\frac{\alpha}{2}\right) a_1 + jCa_2 \tag{20}$$

$$\frac{\partial a_2}{\partial z} = -j\beta a_2 - \left(\frac{\alpha}{2}\right) a_2 + jCa_1 \tag{21}$$

which describes a lossy linear directional coupler, similar to (9) and (10), but now the nonlinearity term is only included in the coupling coefficient C. The initial conditions used are

$$a_1 = \sqrt{\frac{P_{in}}{\text{Area}}} = \sqrt{I_{tot}} \tag{22}$$

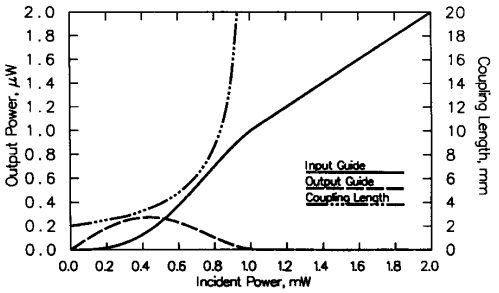

Fig. 4. Theoretical calculations showing switching of a nonlinear coupler of length L_c from a crossed-over state to a straight-through state. Also shown is the dramatic increase in the coupling length around the critical intensity.

$$a_2 = 0 \tag{23}$$

$$\varphi_1 = 0 \tag{24}$$

$$\varphi_2 = -\frac{\pi}{2} \tag{25}$$

where the phase difference between the modes allows the condition that all light excitation is initially in guide 1. These equations are solved by using a 4th-order Runge–Kutta numerical integration to show how the wave propagates down the coupler. Initial excitation power can be varied to show the switching behavior.

Fig. 4 shows a theoretical calculation of the switching behavior of a coupler of length L_c. Note that at low power, all the light is coupled to the output guide. As the power increases, the nonlinear term in the coupling coefficient becomes significant, and C moves toward zero ($L_c \rightarrow \infty$). The effective coupling length is superimposed on Fig. 4, which shows how dramatically the coupling length approaches infinity as the input power rises near the critical power. Note that at higher input powers, the coupler is switched to a straight-through condition as the coupling length increases, where all the light remains in the input guide. It should be noted that the coupling length behavior shown in Fig. 4 is very similar to the recent modeling from Cada [9] using a supermode approach.

Shown in Fig. 5 is the modeled switching behavior of the coupler which was measured. The plots are obtained by multiplying the normalized outputs a_1 and a_2, obtained from the theoretical modeling, by the intensity profiles in the five regions of the linear coupler when modeled as slab waveguides at the 50% crossover point [Fig. 3(b)]. The discontinuity in the center of the plots is due to this representation. The effective coupling length is taken to be $2.73 \times L_c$. In Fig. 5(a), n_2 and α are taken to be zero, the low power state. Therefore, it behaves as a simple linear coupler. In Fig. 5(b), the loss α is introduced to make it a lossy linear directional coupler. Note that the coupling behavior is unaffected. In Fig. 5(c), the nonlinearity n_2 is introduced to represent a lossless nonlinear directional coupler, the high power state. Note, that with high nonlinearity and no loss, a complete straight-through condition is realized. This is due to the lowering of the refractive index in the coupling region MQW and, consequently, a quenching of the evanescent wave coupling to the other guide. Thus, as our theory shows, the effective coupling length increases to infinity. In Fig. 5(d), a more realistic situation with $n_2 \neq 0$ and $\alpha \neq 0$, a lossy nonlinear directional coupler, is displayed where the nonlinearity restrains coupling in a short "active" region of the coupler at the input end. But absorption effects soon lower the high power below the critical intensity, and the remainder of the coupler returns to a quasi-linear coupler. Note, however, that sufficient nonlinear "back-coupling" occurred to effectively switch the output power from guide 2 to guide 1. By varying the input power, the length of the active region of the coupler can be modulated to switch the coupler output signals.

Fig. 6 more clearly shows the active region of the coupler where the coupling in the high power state is retarded for about 0.8 mm. Beyond the initial 0.8 mm distance, the absorption within the coupler has lowered the guided power below a critical power where significant nonlinear effects are realized. The remaining coupler length acts as a linear coupler, but the nonlinearity has effectively switched the output from the upper (output) guide back to the lower or initially inserted guide.

III. Experimental Techniques

The coupler structure, the schematic of which is shown in Fig. 7(a), was grown by molecular beam epitaxy (MBE). The substrate temperature was held at 630°C, as measured by an infrared pyrometer. The entire structure is undoped, and under our growth conditions we measure $p = 1 \times 10^{14}$ in GaAs at 300 K. Photoluminescence measurements were made using an Argon ion laser (5314 Å) and a 1 m Jarell–Ash scanning spectrometer. The room temperature photoluminescence of the MQW region is shown in Fig. 8 and shows strong excitonic behavior.

Initially, the coupler was recessed at the input end about 0.5 mm by removing the upper guide with $NH_4OH : H_2O_2 : H_2O$ (40 : 14 : 970). The coupler was defined by photolithography using a 2 μm mask and AZ 5214 resist. By using an image reversal process, an optimum resist profile was obtained for vertical etches, but the lateral dimensions expanded to 2.5 μm. The coupler was reactive ion etched in a $BCl_3 : Ar$ plasma which gives smooth vertical walls. Vertical walls are critical for this device to be a symmetric coupler. The guides were then protected with plasma enhanced chemical vapor deposition (PECVD) SiO_2 for structural support during lapping and cleaving. A scanning electron microscope (SEM) micrograph of the device is shown in Fig. 7(b).

Measurements were made using a Spectra-Physics Ti : sapphire laser with tunability from 650 nm to 1.1 μm pumped with a Coherent argon ion multiline laser with the capability of delivering up to 20 W of power. The output power of the Ti : sapphire laser was fairly constant with change in wavelength for the region of interest. Laser light was spatially filtered and end coupled into the lower waveguide. Input power was modified by a variable neutral density filter. Input power was measured by a thermal detector with a fairly flat response over the wavelengths (7900–8400 Å) employed here. Output power was measured by focusing the output signal onto a Newport Si detector. Focusing allowed the scattered light to be separated from the main signal.

Waveguide switching was monitored by routing the output signal through a Y branch and having 2% of the light fall on an infrared sensitive camera. The image was displayed on a TV monitor and recorded with an oscilloscope camera. These pictures were then digitized into a 480 × 480 array on the computer. By drawing a rectangle in the digitized image around each waveguide and integrating the pixels while thresholding to suppress the background, an accurate measure of the relative pow-

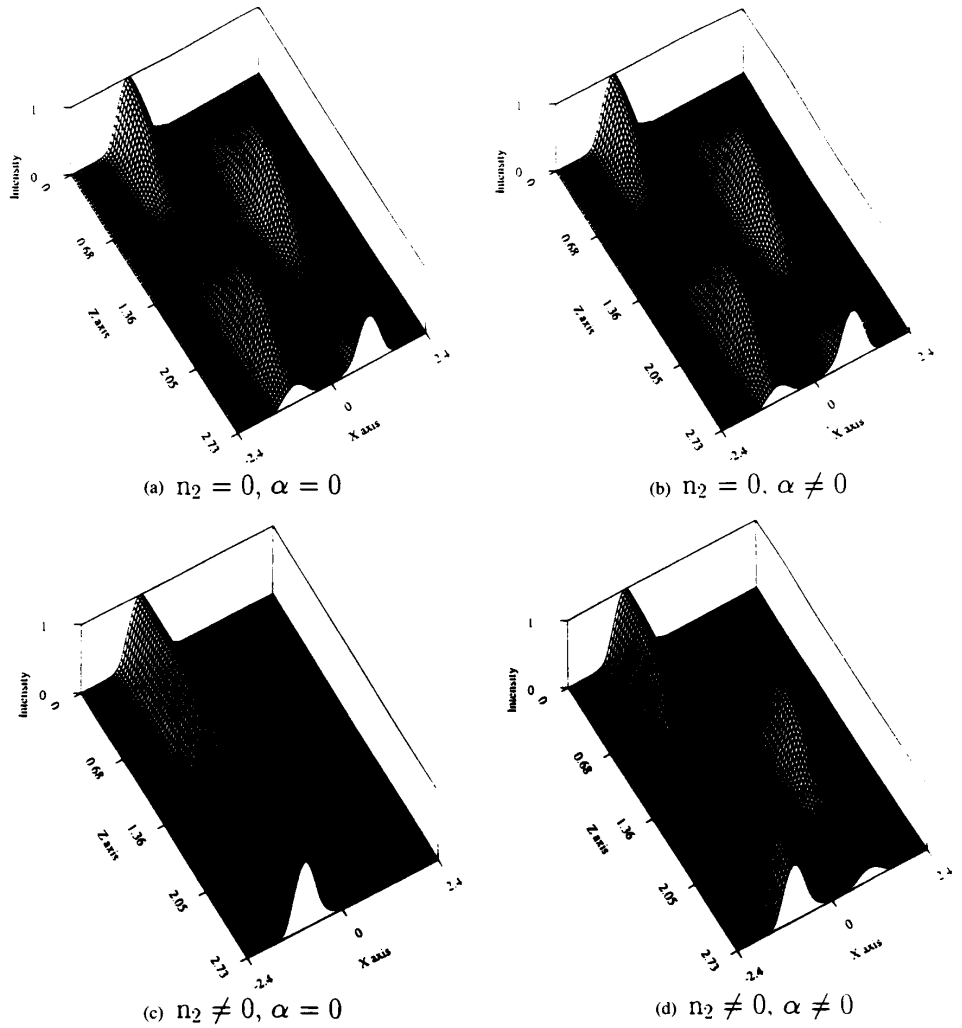

Fig. 5. Modeling of a nonlinear coupler as (a) a lossless linear directional coupler, (b) a lossy linear directional coupler, (c) a lossless nonlinear coupler exhibiting straight-through condition, and (d) a lossy nonlinear coupler where the nonlinearity is overcome by losses and returns to a linear coupler after some length.

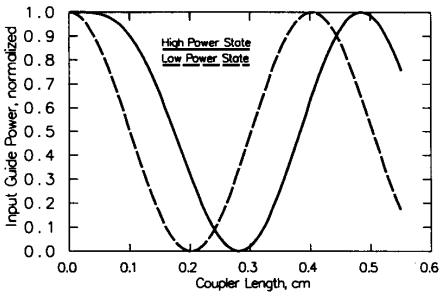

Fig. 6. Modeling of the nonlinear coupler at low and high power states where, at high power, the nonlinearity retards coupling for about 0.8 mm, at which point absorption losses effectively lower the guided power below a critical power and high power state lags the low power state for the remaining coupler distance.

ers in each waveguide could be found. Exact power levels in each guide are calculated by multiplication of the fraction in the guide by the measured power of the Si detector.

Temporal measurements were made with excitation provided by a tunable Coherent dye laser (Styryl-9) in the wavelength range 7800–9000 Å producing 5 ps pulses. The dye laser was pumped with 100 ps mode-locked pulses from a Quantronix Nd:YAG laser frequency doubled with a KDP crystal to 5320 Å. The output from the two channels of the coupler was simultaneously focused onto a Hamamatsu streak camera having a resolution of 10 ps.

IV. Results and Discussion

The waveguides were first characterized with a 20 mW AlGaAs laser. By successive cleaving, the coupling length was found to be vary between 2 and 2.2 mm, in close agreement to

1.0μm	$Al_{0.30}Ga_{0.70}As$	Undoped
0.8μm	$Al_{0.20}Ga_{0.80}As$	Undoped
1.2μm	40 Å GaAs/ 160 Å $Al_{0.3}Ga_{0.7}As$	Undoped
0.8 μm	$Al_{0.20}Ga_{0.80}As$	Undoped
1.0 μm	$Al_{0.30}Ga_{0.70}As$	Undoped
30 prd MQW	50 Å GaAs/50 Å $Al_{0.3}Ga_{0.7}As$	Undoped
Undoped GaAs Substrate		

(a)

(b)

Fig. 7. (a) Schematic of vertical directional coupler with nonlinear coupling medium grown by molecular beam epitaxy, and (b) SEM photomicrograph of the waveguiding structure with PECVD SiO_2 coating for structural support.

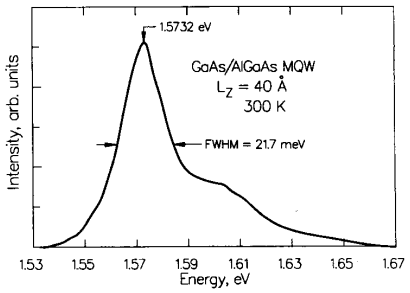

Fig. 8. Room temperature photoluminescence of the multiple quantum well coupling region.

the linear coupling modeling. A 5.5 mm coupler was then measured, taken to be 2.73 × L_c, by varying the input power on the Ti:sapphire laser. Most of the light output is initially coupled over to the upper waveguide at low input powers, but with increasing power, the light output is changed to a straight-through condition. Fig. 9(a) shows the normalized switching behavior, and Fig. 9(b) shows the actual power switching. This coupler exhibited clean single-mode behavior. The solid curves shown are calculated from our theory and show good agreement. The values for the nonlinear refractive index, $n_2 = 1.88 \times 10^{-8}$ cm^2/W, and the loss coefficient, $\alpha = 12.9$ cm^{-1}, were used. The experimental data deviate from our theory at higher powers due to a constant attenuation α being used in the calculations. In reality, as the nonlinearity in the coupling region increases, its effective refractive index is reduced, thus quenching the evanescent wave into the MQW. Since the main loss mechanism is from the coupling region, this lowers the overall attenuation at high nonlinearity. Thus, the measured points at higher power actually see less loss than the theoretical curves predicts.

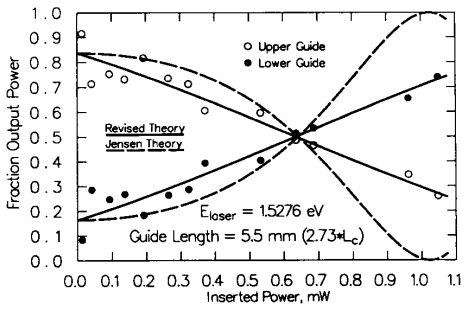

(a)

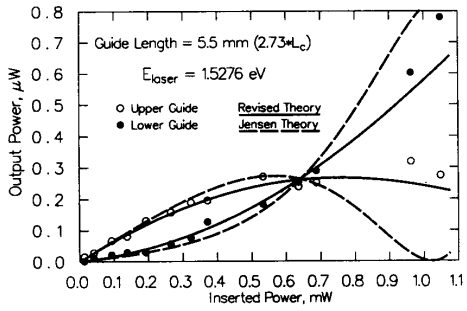

(b)

Fig. 9. Normalized power output of coupler exhibiting a crossed state at elevated powers for energy 45.6 meV below exciton with length 2.73 × L_c (a) and measured power output of same structure (b). Curves shown are theoretical calculations using $n_2 = 1.88 \times 10^{-8}$ and $\alpha = 12.9$ as fitting parameters.

Theoretical modeling using Jensen's theory is also superimposed (dashed lines), on Fig. 9(a) and (b), and shows the switching behavior is similar to the experimental data, but does not clearly model the switching behavior as accurately as our modified theory. The values used in the Jensen model for the nonlinear refractive index and the loss coefficient were $n_2 = 4.65 \times 10^{-9}$ cm^2/W and $\alpha = 12.9$ cm^{-1}. The small value obtained for n_2 is probably because Jensen's theory assumes the nonlinear refractive index is constant throughout the entire coupler; and since our structure confines the nonlinearity to the coupling region alone, the effective n_2 found is smaller.

In Fig. 10(a), the laser wavelength of the Ti:sapphire laser was varied while measuring the total output power from both waveguides of a 2.8 mm length (1.29 × L_c). A large decrease in output power is seen as the energy nears the absorption edge. Inserted power is estimated to be about 850 μW, and is assumed constant over the entire scanned wavelength region. The coupling behavior was also monitored, and the upper or "output" guide normalized output is shown in Fig. 10(b). Note that at smaller energies, far from band edge, most of the light is coupled over to the upper guide. As the energy is increased, it is expected that the absorption and nonlinearity should increase. In Fig. 10(b), as the energy increases, the coupler is moving toward the straight-through condition, perhaps due to increasing nonlinearity. The curves shown are fit to aid the eye. Eventually, the coupler returns to the quasi-linear coupling behavior, similar to the lower energy coupling. This might be due to increasing absorption overtaking the increasing nonlinearity. However, the data here appear more noisy probably since this sample showed single-mode and sometimes double-mode be-

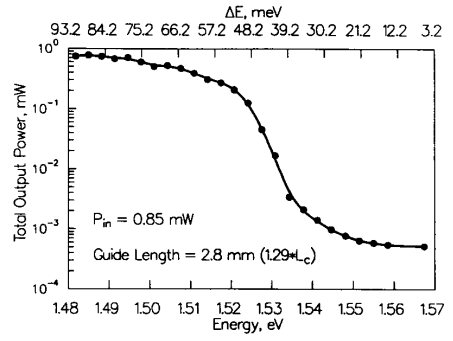

Fig. 10. (a) Transmission of the nonlinear coupler at energies below exciton, and (b) output guide normalized power behavior.

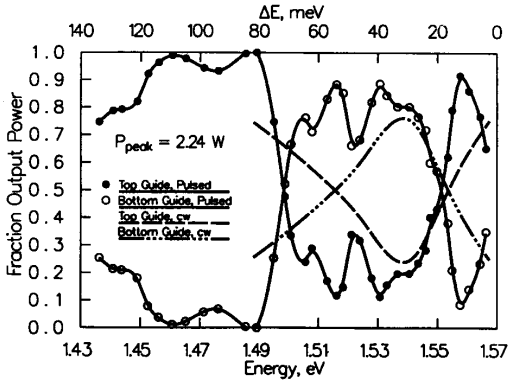

Fig. 11. Transmission of the nonlinear coupler with high peak power laser pulses.

havior, due to the slightly wider waveguide dimensions after delineation. Exact explanations near the band gap may, however, be harder to extract.

Fig. 11 shows the normalized output (amplitude) from the two channels of a 2.8 mm (1.29 × L_c) coupler sample recorded by the streak camera, due to pulsed (5 ps) excitation from a dye laser (solid lines). The peak power of the dye laser pulses (2.24 W) is several orders of magnitude higher than the Ti : sapphire CW input. Thus, Fig. 11 shows similar switching behavior with photon energy as in Fig. 10(b) (superimposed as the dashed lines in Fig. 11), but the higher power pulses shifts the first crossover point to lower photon energy. Fig. 11 also demonstrates the three switched state regions. At low energy, we have a crossover state, and then a dramatic switch to the straight-through state at about 1.50 eV. The straight-through condition persisted for a region of 1.50–1.555 eV, but then it seems absorption effects at energies closer to the band edge begin to restore the coupler to a crossover state. In studying the temporal behavior (relative to one another) of the output of the two guides, we find that there is no delay at lower excitation (regions 1 and 2). But, in the third region where crossover was maintained above ~ 1.555 eV till cutoff occurred, a measurable delay of ~ 10–12 ps was observed between the two channels. This delay is perhaps indicative of room temperature excitonic polaritons in the GaAs–AlGaAs MQW propagating parallel to the quantum well layer [13].

It should be mentioned that the main contribution of the nonlinearity is expected to be an optical effect near the band edge and not a thermal nonlinearity. Li Kam Wa *et al.* [5], using a Mach–Zehnder interferometer, showed that the thermal nonlinearity is positive and the optical nonlinearity is negative, and the net result Li Kam Wa *et al.* demonstrated was a negative nonlinearity. Using high peak power and/or high repetition rates of pulsed lasers, there may be some cancelling of thermal and optical nonlinearity. However, in our case, the CW laser power inserted was fairly low (~ 1 mW), below which thermal effects should dominate. Also, Fig. 10(b) (also dashed lines in Fig. 11) obtained using a CW laser shows the same three switching regimes shown in Fig. 11 (solid lines) obtained using a low repetition rate (76 MHz) pulsed laser. The switching in Fig. 11 between regions 1 and 2 occurs at lower energy, further from band edge than Fig. 10(b), since the peak power of the pulses is several orders of magnitude larger. Since thermal effects are not expected with the pulsed laser and both curves are similar, optical nonlinearity is expected to be the dominant mechanism.

V. Conclusion

A device which clearly demonstrates all-optical switching is analyzed and measured. It exhibits nonlinear switching and low loss. Table I shows a comparison to previously reported nonlinear directional couplers. Some of the values shown were obtained from a conversion to a common set of units to facilitate comparison. The first two devices were made by Li Kam Wa *et al.* [2]–[5]. The loss varies according to the ΔE (energy below band edge); but for comparable ΔE, it is estimated that losses of these devices are larger than our vertical scheme. Das *et al.* [14] demonstrated a strained layer InGaAs–GaAs coplanar directional coupler which was measured by interferometric methods. Their loss was even greater, probably due to recombination and increased scattering at the strained-layer interfaces. Cada *et al.* [8] have demonstrated switching in vertical nonlinear slab waveguides, but did not analyze their experimental results.

It appears that coplanar couplers in which all five regions are nonlinear have higher loss but also higher nonlinearity (n_2); but this is perhaps because modeling the vertical structure with Jensen's theory assumes a constant n_2 throughout the coupler, thus the greatly reduced overall nonlinear index of refraction (n_2 = 4.65×10^{-9}). Our model predicts a larger nonlinear refractive

TABLE I
COMPARISON OF TESTED NONLINEAR DIRECTIONAL COUPLERS

Type of Coupler	Coplanar GaAs–AlGaAs MQW [3]	Coplanar GaAs–AlGaAs MQW [3]	Coplanar InGaAs–GaAs SLS [12]	Vertical GaAs–AlGaAs MQW
ΔE (meV)	51.9 (PL)	36.9 (PL)	~40 (Abs)	45.6 (PL)
α (cm^{-1})	13.5	~20	30	12.9
I_c (W/cm^2)	5×10^{4}[a]	N/A	1×10^{4}	3×10^{4}
n_2 (cm^2/W)	1×10^{-7}	$\sim 1.3 \times 10^{-7}$	2.25×10^{-7}	1.88×10^{-8} (4.65×10^{-9})[b]

N/A—not available.
[a]Estimated.
[b]Jensen theory.

index ($n_2 = 1.88 \times 10^{-8}$), but may not be as meaningful since our hypothesis of the coupling coefficient C does not start from a physical material representation.

The advantage of our analysis is that it more suitably models the nonlinear effect in couplers with only nonlinear coupling medium since, physically, we believe the nonlinearity manifests itself differently. In our case, we believe the evanescent tail to the opposite guide is being modulated, rather than the phases φ_1 and φ_2. As proof, our analysis agrees more closely with the experimental data.

ACKNOWLEDGMENT

The authors would like to thank J. Fournier for his help during reactive ion etching and J. Pamulapati for help in growing the heterostructures by molecular beam epitaxy.

REFERENCES

[1] S. M. Jensen, "The nonlinear coherent coupler," *IEEE J. Quantum Electron.*, vol. QE-18, pp. 1580–1583, 1982.
[2] P. Li Kam Wa, J. E. Sitch, N. J. Mason, J. S. Roberts, and P. N. Robson, "All optical multiple-quantum well waveguide switch," *Electron. Lett.*, vol. 21, pp. 26–27, 1985.
[3] P. Li Kam Wa, J. H. Marsh, P. N. Robson, J. S. Roberts, and N. J. Mason, "Nonlinear propagation in GaAs/GaAlAs multiple quantum well waveguides," in *Proc. SPIE*, vol. 578, Boston, MA, 1985.
[4] P. Li Kam Wa, P. N. Robson, J. P. R. David, G. Hill, P. Mistry, M. A. Pate, and J. S. Roberts, "All-optical switching effects in a passive GaAs/GaAlAs multiple quantum well waveguide resonator," *Electron. Lett.*, vol. 22, pp. 1129–1130, 1986.
[5] P. Li Kam Wa and P. N. Robson, "Nonlinear multiple quantum well waveguide devices," *Proc. SPIE*, vol. 800, Novel Optoelectron. Devices, pp. 43–49, 1987.
[6] D. A. B. Miller, D. S. Chemla, D. J. Eilenberger, P. W. Smith, A. C. Gossard, and W. T. Tsang, "Large room-temperature optical nonlinearity in GaAs/$Al_{1-x}Al_xAs$ multiple quantum well structures," *Appl. Phys. Lett.*, vol. 41, pp. 679–681, 1982.
[7] M. Cada, R. C. Gauthier, B. E. Paton, and J. Chrostowski, "Nonlinear guided waves coupled nonlinearly in a planar GaAs/GaAlAs multiple quantum well structures," *Appl. Phys. Lett.*, vol. 49, pp. 755–757, 1986.
[8] M. Cada, B. P. Keyworth, J. M. Glinski, A. J. Springthorpe, and P. Mandeville, "Experiment with multiple-quantum well waveguide switching element," *J. Opt. Soc. Amer. B*, vol. 5, pp. 462–466, 1988.
[9] M. Cada and J. D. Begin, "An analysis of a planar optical directional coupler with a lossless Kerr-like coupling medium," *IEEE J. Quantum Electron.*, vol. 26, pp. 361–371, 1990.
[10] P. Berger, Y. Chen, P. Bhattacharya, J. Pamulapati, and G. C. Vezzoli, "Demonstration of all-optical modulation in a vertical guided-wave nonlinear coupler," *Appl. Phys. Lett.*, vol. 52, pp. 1125–1127, 1988.
[11] D. Marcuse, "Directional couplers made in nonidentical asymmetric slabs. Part I: Synchronous couplers," *J. Lightwave Technol.*, vol. LT-5, pp. 113–118, 1987.
[12] S. Adachi, "GaAs, AlAs, and $Al_xGa_{1-x}As$: Material parameters for use in research and device applications," *J. Appl. Phys.*, vol. 58, pp. R1–R29, 1987.
[13] K. Ogawa, T. Katsuyama, and H. Nakamura, "Time-of-flight measurement of excitonic polaritons in a GaAs/AlGaAs quantum well," *Appl. Phys. Lett.*, vol. 53, pp. 1077–1079, 1988.
[14] U. Das, Y. Chen, and P. Bhattacharya, "Nonlinear effects in coplaner GaAs/InGaAs strained-layer superlattice directional couplers," *Appl. Phys. Lett.*, vol. 51, pp. 1679–1681, 1987.

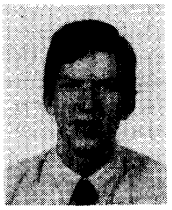

Paul R. Berger (S'84–M'91) received the B.S.E. degree in engineering physics in 1985, and the M.S.E. and Ph.D. degrees in electrical engineering in 1987 and 1990, respectively, all from the University of Michigan, Ann Arbor. His Ph.D. dissertation studied MBE growth kinetics of strained III–V semiconductors using RHEED, MBE selective area regrowth, and the application of these to monolithically integrated optoelectronics including guided-wave detectors/modulators and photoreceivers.

Since August 1990 he has been employed as a Postdoctorate at AT&T Bell Laboratories, Murray Hill, NJ, in the Optoelectronic Device Research Department. His current research interests include semiconductor lasers and monolithic integration of optoelectronic devices.

Dr. Berger is a member of the Optical Society of America.

Pallab K. Bhattacharya (M'78–SM'83–F'89), for a photograph and biography, see this issue, p. 768.

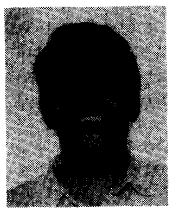

Shantanu Gupta was born in Calcutta, India, in 1965. He received the B.Tech. degree in electrical engineering from the Indian Institute of Technology, Kanpur, in 1986, and the M.S. degree in electrical engineering from the University of Rochester, Rochester, NY, in 1988.

Since 1988 he has been working toward the Ph.D. degree in electrical engineering at the University of Michigan, Ann Arbor. He has worked on the generation, detection, and application of subpicosecond electrical pulses in III–V semiconductors. Currently he is studying ultrafast phenomena in III–V semiconductors using femtosecond laser techniques. His research also includes the study of femtosecond optical interactions in fibers in the 1.5 μm wavelength region.